

# Critical slowing down anticipates emergence and elimination of measles in Niger

Andrew T. Tredennick<sup>1,2\*</sup>, Eamon O’Dea<sup>1,2</sup>, Andrew W. Park<sup>1,2</sup>, Tobias Brett<sup>1,2</sup>, Matthew J. Ferrari<sup>3</sup>,  
Pejman Rohani<sup>1,2</sup>, & John M. Drake<sup>1,2</sup>

<sup>1</sup> *Odum School of Ecology, University of Georgia, Athens, GA, USA*

<sup>2</sup> *Center for the Ecology of Infectious Diseases, University of Georgia, Athens, GA, USA*

<sup>3</sup> *Department of Biology, Pennsylvania State University, State College, PA, USA*

## Abstract

### 1 Introduction

2 Theory shows that epidemic transitions can be anticipated by trends in the statistical properties of disease  
3 time series (AERO papers). The existence of statistical trends in the data that precede critical transitions,  
4 so-called ‘early warning signals’ (EWS), imply that we may be able to anticipate disease emergence and  
5 outbreaks. The end goal is a model-independent detection system, where statistical properties of disease  
6 surveillance data can trigger warnings of impending outbreaks without the need to fit mechanistic models of  
7 disease transmission (Han and Drake 2016).

8 However, there is currently a gap between the theoretical work, which has relied on knowing the underlying  
9 disease dynamics, and the eventual goal of applying EWS in real-world situations where the underlying  
10 disease dynamics may be unknown. Theoretical development of EWS has focused on anticipating when the  
11 population becomes supercritical, when  $R_0 > 1$ , after which an outbreak is inevitable, perhaps with some  
12 bifurcation delay (Dibble et al. 2016). Knowing the value of  $R_0$  through time makes it possible to test the  
13 accuracy of EWS that are estimated from state variables alone. Empirical application of EWS does not  
14 require knowing the value of  $R_0$  through time, meaning that “tests” require making assumptions about when  
15 critical transitions occur. Whether EWS anticipate critical transitions in real disease time series remains  
16 unknown, and is a critical knowledge gap that must be filled before EWS can confidently be deployed.

17 Here, we use empirically-based model simulations of measles dynamics to test whether EWS anticipate  
18 critical transitions in realistic disease dynamics. Our focus is on the re-emergence of measles following a  
19 large outbreak, a situation typical of measles dynamics in sub-Saharan Africa. We seek to answer two related  
20 questions. First, can EWS distinguish between time series of disease incidence when the underlying  
21 dynamics are far from and near to a critical transition? If so, then EWS can anticipate disease re-emergence  
22 and large outbreaks. Second, how does the distance to and the rate of approaching the epidemic threshold  
23 impact the performance of EWS? It may be that some EWS perform well when disease re-emergence is slow,  
24 while others perform well when the epidemic threshold is rapidly reached.

---

\*Corresponding author: atredenn@gmail.com

To answer these questions, we fit mechanistic models of disease transmission to time series of measles incidence in four Nigerien cities: Agadez, Maradi, Niamey, and Zinder. We then use the fitted models to perform model experiments designed to test the performance of EWS at anticipating critical transitions after susceptible depletion. Our results confirm theoretical expectations about several EWS. In particular, we show that several EWS anticipate critical transitions in realistic scenarios, and they do so using much shorter time series than used in theoretical studies. However, our study also highlights the limitations of EWS in situations where disease re-emergence occurs rapidly.

## Materials and Methods

### Data

We used weekly measles case report data from four Nigerien cities, collected over an 11 year period (1995-2005) (Figure 1). These data are ideal for stress testing EWS because each city has different population sizes, has different dynamics in terms of size of outbreaks and length of inter-epidemic periods, and each time series has different amounts of demographic stochasticity due to differences in population size. The data come from [somewhere/someone], and used here with permission from [somewhere/someone].

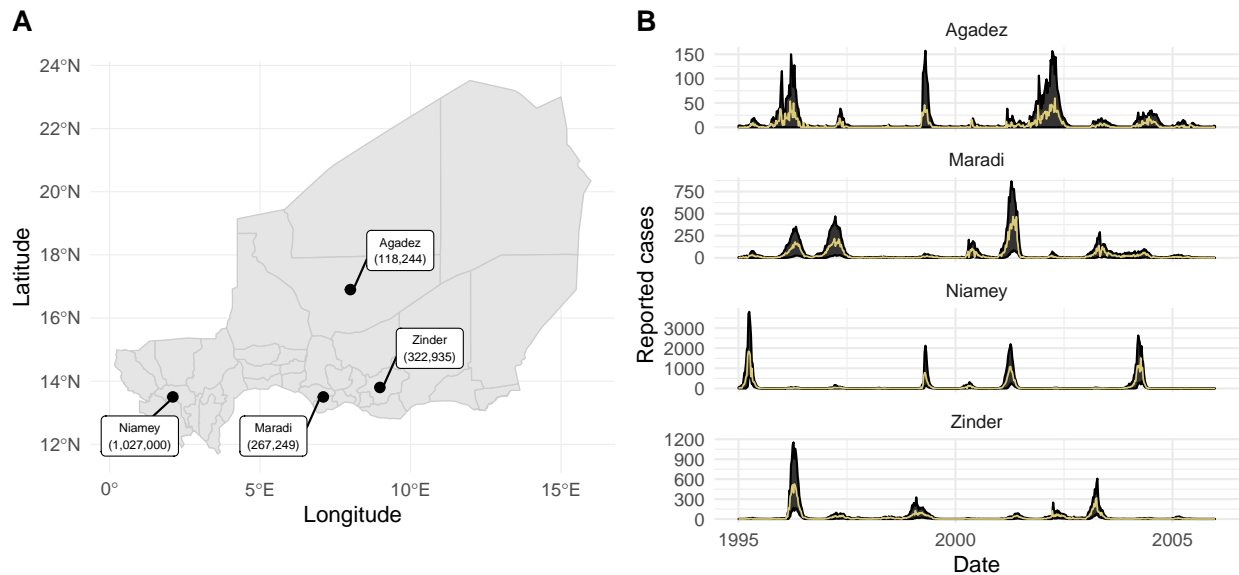


**Figure 1:** (A) Locations and population sizes (in parantheses) of our four focal cities in Niger. (B) Time series of reported cases (yellow solid lines) and the 95% prediction intervals (black ribbons) for one-step-ahead forecasts from our fitted SEIR models for each city.

### Stochastic SEIR model

The model is a discrete-time approximation of a continuous-time SEIR model with limited demography, specified as a set of difference equations,

$$S_{t+dt} = n_{S,t} - n_{E,t} \quad (1)$$

$$E_{t+dt} = n_{E,t} - n_{I,t} \quad (2)$$

$$I_{t+dt} = n_{I,t} + n_{O,t} - n_{R,t}, \quad (3)$$

where  $\mathbf{n}_t$  are random variables representing the number of individuals transitioning into or out of each class at each timestep  $t \rightarrow t + dt$ .  $n_S$  is the number of births,  $n_E$  is the number of newly infected individuals that have the disease but are not infectious,  $n_I$  is the number of newly infectious individuals,  $n_O$  is the number of imported infections, and  $n_R$  is the number of newly recovered individuals who are no longer infectious and have life-long immunity. The stochastic random variables are specified as follows:

$$n_{S,t} \sim \text{Poisson}(\mu_t N_t \times dt) \quad (4)$$

$$n_{E,t} \sim \text{Binomial}(\lambda_{E,t}, S_t) \quad (5)$$

$$n_{I,t} \sim \text{Binomial}(\lambda_{I,t}, E_t) \quad (6)$$

$$n_{O,t} \sim \text{Poisson}(\psi \times dt) \quad (7)$$

$$n_{R,t} \sim \text{Binomial}(\lambda_{R,t}, I_t), \quad (8)$$

where  $\mu_t$  is the birth rate at time  $t$ ,  $\psi$  is the rate of imported infections, and  $\lambda_E$ ,  $\lambda_I$ , and  $\lambda_R$  are the probabilities of exposure, becoming infectious, and recovery, respectively. These probabilities reflect the processes of transmission, transition from the latent period to the infectious period, and recovery, which we model as:

$$\lambda_{E,t} = 1 - e^{-\frac{\beta_t I_t dt}{N_t}} \quad (9)$$

$$\lambda_{I,t} = 1 - e^{-\eta E_t dt} \quad (10)$$

$$\lambda_{R,t} = 1 - e^{-\gamma I_t dt}, \quad (11)$$

where  $\beta_t$  is time-varying rate of transmission,  $\eta$  is time-invariant rate from the exposed class to the infectious class, and  $\gamma$  is time-invariant recovery rate. We model rate of transmission as:

$$\beta_t = \beta \left( 1 + \sum_{i=1}^6 q_i \xi_{i,t} \right) \Gamma_t. \quad (12)$$

$\beta$  is the mean transmission rate,  $\psi$  accounts for measles infections from external sources that are not part of the local dynamics, and the term  $\sum_{i=1}^6 q_i \xi_{i,t}$  is a B-spline to model seasonality in transmission. The B-spline bases ( $\xi_{i,t}$ ) are periodic with a 1 year period. The transmission rate ( $\beta_t$ ) is also subject to stochastic process noise at each time step,  $\Gamma_t$ , which we model as a gamma-distributed white (temporally uncorrelated) noise with mean 1 and variance  $\sigma^2$  (Bretó and Ionides 2011).

We do not include a death process in the model because the rate of infection is much faster than the rate of death. Excluding deaths means we can avoid making further assumptions about demographic rates – we are already making assumptions about birth rates (e.g., the rate is the same across cities, but with city-specific population size). We model demographic stochasticity in births and imported infections by drawing

time-specific values from Poisson distributions. Transitions in the model are shown in Table 1. In this model, the effective reproductive ratio at time  $t$  is:  $R_E(t) = \frac{\beta_t S_t}{\gamma N_t}$ . We assume observed case reports ( $\mathbf{y}$ ) are drawn from a Negative Binomial distribution subject to a constant reporting fraction ( $\rho$ ) and dispersion parameter  $\tau$ ,

$$y_t \sim \text{Negative Binomial}(\rho I_t, \tau). \quad (13)$$

**Table 1:** Transitions in the SEIR model. We show the deterministic transmission rate for clarity, but our model uses the stochastic transmission rate.

Transition	$(\Delta S, \Delta E, \Delta I)$	Propensity
birth	$(1, 0, 0)$	$N_t \mu_t$
transmission (deterministic)	$(-1, 1, 0)$	$SI\beta_t/N_t$
transmission (stochastic)	$(-k, k, 0)$	$\frac{S}{k} \sum_{j=0}^k \binom{k}{j} (-1)^{k-j+1} \tau_f^{-1} \ln(1 + (\beta_t I/N_t)) \tau_f (S - j)$
symptomatic (infectious)	$(0, -1, 1)$	$E\eta$
imported infections	$(0, 0, 1)$	$\psi_t$
recovery	$(0, 0, -1)$	$I\gamma$

## Model fitting and inference

We fit the SEIR model to time series of case reports from each of our focal cities using Maximization by Iterated particle Filtering (MIF). We estimated 14 parameters for each city: six seasonal transmission parameters ( $q_i$ ), mean transmission rate ( $\beta$ ), three initial conditions ( $S_{(t=0)}, E_{(t=0)}, I_{(t=0)}$ ), the number of imported infections ( $\psi$ ), reporting fraction ( $\rho$ ), one parameter accounting for process noise ( $\sigma$ ), and one parameter accounting for measurement noise ( $\tau$ ). To ensure identifiability, and to make the model easier to fit, we assumed the infectious period was fixed at  $1/\eta = 8$  days and the recovery period was fixed at  $1/\gamma = 5$  days. The birth rate ( $\mu_t$ ) was multiplied by 0.3 to account for the reported 70% vaccination coverage (Ferrari et al. 2008).

MIF relies on particle filtering, which estimates the likelihood of fixed parameters by integrating state variables of a stochastic system. To narrow in on the maximum likelihood estimates, MIF lets parameters take a random walk during the filtering process and selectively propagates forward parameter sets (i.e., particles) with the highest likelihood. The variance of the random walk decreases at each iteration of MIF, where a MIF iteration means one filtering pass through the time series. This procedure converges toward the maximum likelihood estimates (MLEs), in theory.

We used the IF2 algorithm (Ionides et al. 2015) implemented in the R (R Core Team 2017) package pomp (King et al. 2016, 2018) to conduct the MIF procedure. To initialize MIF, we generated 5000 parameter sets using Latin Hypercube Sampling over large ranges of the parameter values. We then performed two rounds of MIF, each for 100 iterations, with 10000 particles, and geometric cooling. For the first round of MIF we set `cooling.factor = 1`. For the second round, which was initialized using the collection of parameter

sets from the end of the first round, we set `cooling.factor = 0.9`. We computed the log likelihood of 5000 final MIF parameter sets (i.e., parameter sets collected after 200 MIF iterations) as the log of the mean likelihoods of 50 replicate particle filters with 10000 particles each. At this stage, we assume the parameter set with highest log likelihood is the MLE.

We used profiling to estimate 95% confidence intervals for four parameters of interest: mean transmission rate ( $\beta$ ), the initial fraction of susceptible individuals ( $S_{(t=0)}$ ), the number of imported infections ( $\psi$ ), and reporting fraction ( $\rho$ ). For each parameter, we profiled over a range of 100 values using the same MIF and likelihood estimate procedure as described above for finding the MLEs. We replicated the profiling procedure 10 times for each unique value of the focal parameter and then took the log of the mean of those 10 profiled likelihoods. These values were used to estimate 95% confidence intervals using the Monte Carlo-adjusted profile algorithm described by Ionides et al. (2017).

## Model simulations

We used the MLE parameter sets to make one-step-ahead predictions, to estimate any trend in transmission rate through time, and to test the ability of early warning signals to anticipate the critical transition at  $R_E(t) = 1$ . To make one-step-ahead predictions, we used particle filtering with 50000 particles and retained the mean and standard deviation of all latent across all particles before they were filtered at each time step. To estimate a trend in transmission rate, we allowed mean transmission to take a random walk throughout the filter and retained the filtered distribution of particles for mean transmission and  $R_E(t)$ .

We manipulated the initial size of the susceptible pool to simulate an increase from low  $R_E(t)$  to high  $R_E(t)$ . Doing so allows us to test whether EWS can distinguish between windows of time when  $R_E(t)$  is far from a critical transition and when  $R_E(t)$  is near a critical transition. We reduced the initial fraction of susceptible individuals by multiplying the MLE for  $S_{(t=0)}$  by six discounting factors: 1e-4, 0.1, 0.2, 0.3, 0.4, and 0.5. These discounting factors represent situations of susceptible depletion after outbreaks of various size. We then simulated the model forward for thirty years using mean birth and death rates for the entire country. Thirty years was long enough for yearly average  $R_E(t)$  to reach 1 for each city. Because the model is stochastic, we repeated these simulations 500 times for each city-susceptible discount combination.

Next, we split each simulated time series into null and test intervals. First, across all simulations for a city-susceptible discount combination, we found the simulation year in which yearly average  $R_E(t)$  reached 1, and excluded years past that time. We split the remaining time series into two windows of equal length. The null interval is the first window, where  $R_E(t)$  is increasing but far from 1. The test interval is the second window, where  $R_E(t)$  is increasing and approaching 1. We did this for each city and for each level of susceptible depletion. We calculated EWS over null and test intervals separately, as described next.

## Early warning signals

We considered ten candidate early warning signals. We used the `spaero::get_stats()` function (O’Dea 2018) in R (R Core Team 2017) to calculate EWS according to the formulas in Table 2. All EWS except the coefficient of variation are expected to increase as  $R_E(t)$  approaches 1 (Brett et al. 2018). However, we still include the coefficient of variation because it is often used EWS in other applications.

For each simulation of each city-susceptible discount combination, we calculated each EWS for the time series of expected cases in the null and test intervals. This yields a distribution of EWS over the 500 null and test intervals. The bandwidth for EWS calculation varied because we set  $b$  to be one-half the length of the

interval. That is, we do not use a moving window and if, for example, the length of the interval is 520 weeks (10 years), then  $b = 0.5 \times 520 = 260$ .

We assessed the performance of each EWS using the Area Under the Curve (AUC) statistic. Specifically, we use AUC to calculate the amount of overlap between the distributions of each EWS from the null and test intervals. Higher values of AUC indicate a greater degree of separation and thus better performance of a particular EWS in terms of classifying whether  $R_E(t)$  is approaching a critical transition. We used the `pROC::auc()` function (Robin et al. 2011) in R to calculate AUC values.

**Table 2:** List of candidate early warning signals and their estimating equations. Note that  $b$  denotes the bandwidth. See Brett et al. (2018) for details.

EWS	Estimator	Theoretical Correlation with $R_E(t)$
Mean	$\mu_t = \sum_{s=t-(b-1)\delta}^{t+(b-1)\delta} \frac{X_s}{2b-1}$	Positive
Variance	$\sigma_t^2 = \sum_{s=t-(b-1)\delta}^{t+(b-1)\delta} \frac{(X_s - \mu_s)^2}{2b-1}$	Positive
Coefficient of variation	$CV_t = \frac{\sigma_t}{\mu_t}$	Null
Index of dispersion	$ID_t = \frac{\sigma_t^2}{\mu_t}$	Positive
Skewness	$S_t = \frac{1}{\sigma_t^3} \sum_{s=t-(b-1)\delta}^{t+(b-1)\delta} \frac{(X_s - \mu_s)^3}{2b-1}$	Positive
Kurtosis	$K_t = \frac{1}{\sigma_t^4} \sum_{s=t-(b-1)\delta}^{t+(b-1)\delta} \frac{(X_s - \mu_s)^4}{2b-1}$	Positive
Autocovariance	$ACov_t = \sum_{s=t-(b-1)\delta}^{t+(b-1)\delta} \frac{(X_s - \mu_s)(X_{s-\delta} - \mu_{s-\delta})}{2b-1}$	Positive
Autocorrelation	$AC_t = \frac{ACov_t}{\sigma_t \sigma_{t-\delta}}$	Positive
Decay time	$\bar{\tau}_t = -\delta / \ln[AC_t(\delta)]$	Positive
First differenced variance	$\Delta\sigma_t^2 = \sigma_t^2 - \sigma_{t-\delta}^2$	Positive

## Results

### Model fit and simulations

The fitted models adequately reproduce observed dynamics (Figure 1), with in-sample  $R^2$ s from one-step-ahead predictions ranging from 0.54 for Agadez to 0.89 for Maradi (Figure 2). Stochastic simulations of the models displayed dynamics typical of each city (Figure Sx), including the decline in seasonality amplitude as population size decreases (Figure Sx; Ferrari et al. 2008). Our model for Agadez performs poorly relative to the other cities.

We found no evidence of a directional trend in the rate of transmission over the course of the time series (Figure Sx). Seasonal fluctuations in all cities cause  $R_E(t)$  to go above and below 1 throughout the course of a year (Figure Sx). This results in the observed outbreak cycles in low population cities and the more unpredictable outbreaks in larger cities (Figure 1).

Stochastic simulations from sub-critical ( $R_E(t) \ll 1$ ) to critical dynamics ( $R_E(t) = 1$ ) differed among the four cities (Figure 3). The differences in the rate at which  $R_E(t)$  approaches one is a combination of population size, mean transmission rate, and seasonality (Table 3). For example, the dynamics of Niamey

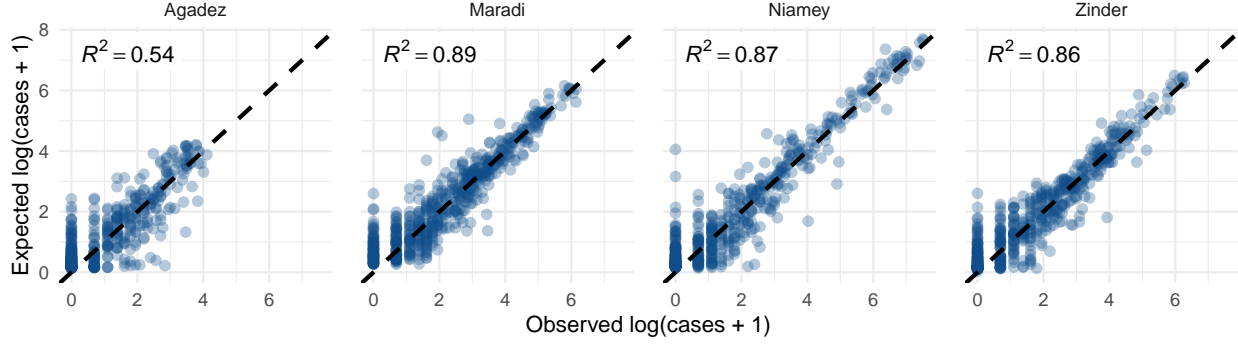


**Figure 2:** Comparison of in-sample model predictions and observations for each city. Expected cases are one-step-ahead predictions from the fitted models. The dashed line shows 1:1.

reach  $R_E(t) = 1$  much faster than the other cities that have smaller populations, lower transmission rates (generally), and lower seasonal amplitude.

**Table 3:** Maximum likelihood estimates for select epidemiological parameters.

City	Log likelihood (S.E.)	$\beta$	$\sigma$	$\psi$	$\rho$	$S_{t=0}$
Agadez	-960.65 (0.11)	171.47	0.10	7.80	0.77	0.23
Maradi	-1746.56 (0.16)	483.09	0.06	24.88	0.33	0.10
Niamey	-1454.73 (0.15)	370.63	0.09	23.28	0.26	0.11
Zinder	-1415.52 (0.09)	180.09	0.08	10.47	0.36	0.22

## Performance of EWS

The EWS generally perform as expected, with Niamey being an exception (Figure 4). Skewness, kurtosis, and coefficient of variation performed poorly across all levels of susceptible depletion in all cities except Niamey. For Niamey, it appears these metrics perform well at the highest levels of susceptible depletion (i.e., low discounting factors). In fact, the high AUC values for Niamey result from exceptionally poor performance: they are all higher in the null interval rather than the test interval, contrary to theoretical expectations (Table 2). Thus, these metrics are unreliable.

For the other cities, variance, mean, index of dispersion, decay time, autocovariance, and autocorrelation all perform equally well (Figure 4). Their performance declines as the amount of susceptible depletion decreases. This is expected because more rapid returns to  $R_E(t) = 1$  result in shorter null and test intervals, making estimates of EWS less precise. Likewise, as the total time to reach  $R_E(t) = 1$  decreases, the null and test intervals start to behave more similarly. In part, this is because susceptible replenishment is linear in our model. Nonlinear increases in the susceptible pool would lead to different dynamics.

## Discussion

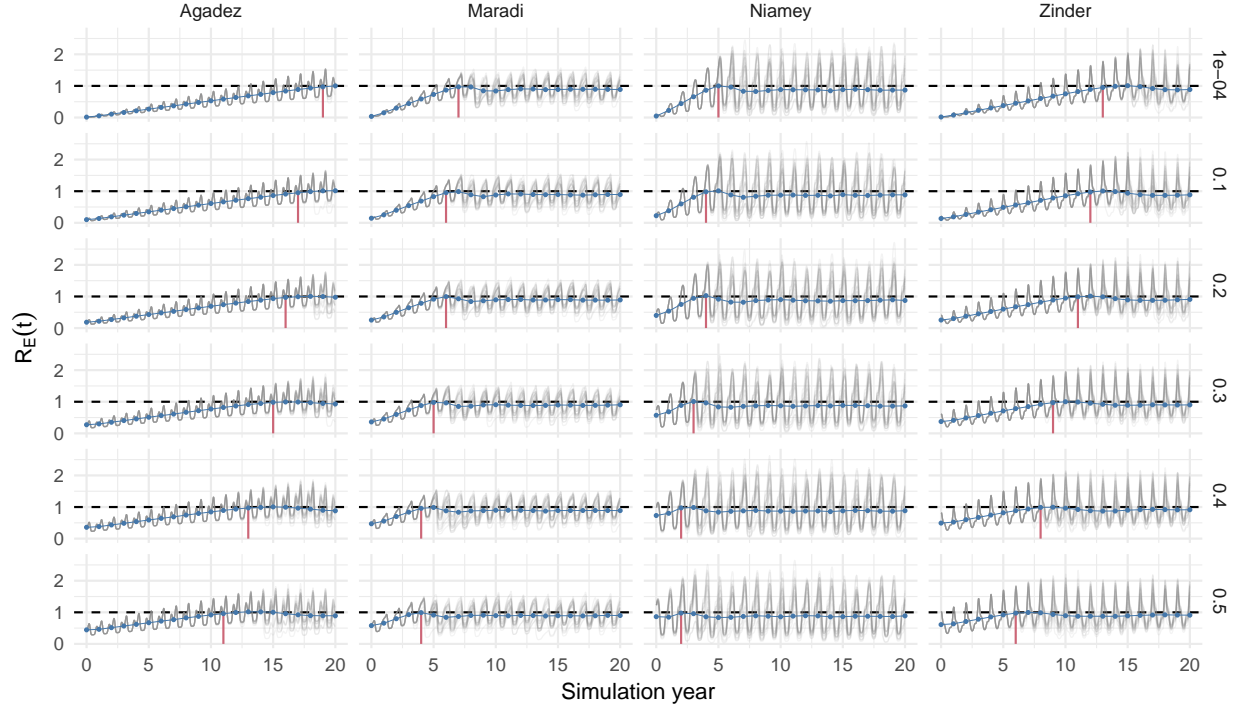


**Figure 3:** Yearly average  $R_E(t)$  (blue lines) across 500 model simulations at the MLE parameters and 20 representations simulations (grey lines) for each city. Each row of panels is for one level of susceptible depletion, indicated by the value on the right-most edge of the plots. The horizontal dashed line shows where  $R_E(t) = 1$ . The vertical solid red lines show the time point at which yearly average  $R_E(t) \geq 1$ . The time periods before the red line for each city were used for testing early warning signals.

## Acknowledgments

This research was funded by the National Institute of General Medical Sciences of the National Institutes of Health (Award Number U01GM110744). The funders had no role in study design, data collection and analysis, decision to publish, or preparation of the manuscript. This work was done on the Olympus High Performance Compute Cluster located at the Pittsburgh Supercomputing Center at Carnegie Mellon University, which is supported by National Institute of General Medical Sciences Modeling Infectious Disease Agent Study (MIDAS) Informatics Services Group grant 1U24GM110707.

## References

- Bretó, C., and E. L. Ionides. 2011. Compound Markov counting processes and their applications to modeling infinitesimally over-dispersed systems. *Stochastic Processes and their Applications* 121:2571–2591.
- Brett, T. S., E. B. O’Dea, É. Marty, P. B. Miller, A. W. Park, J. M. Drake, and P. Rohani. 2018. Anticipating epidemic transitions with imperfect data. *PLoS Computational Biology* 14:e1006204.
- Dibble, C. J., E. B. O’Dea, A. W. Park, and J. M. Drake. 2016. Waiting time to infectious disease emergence.



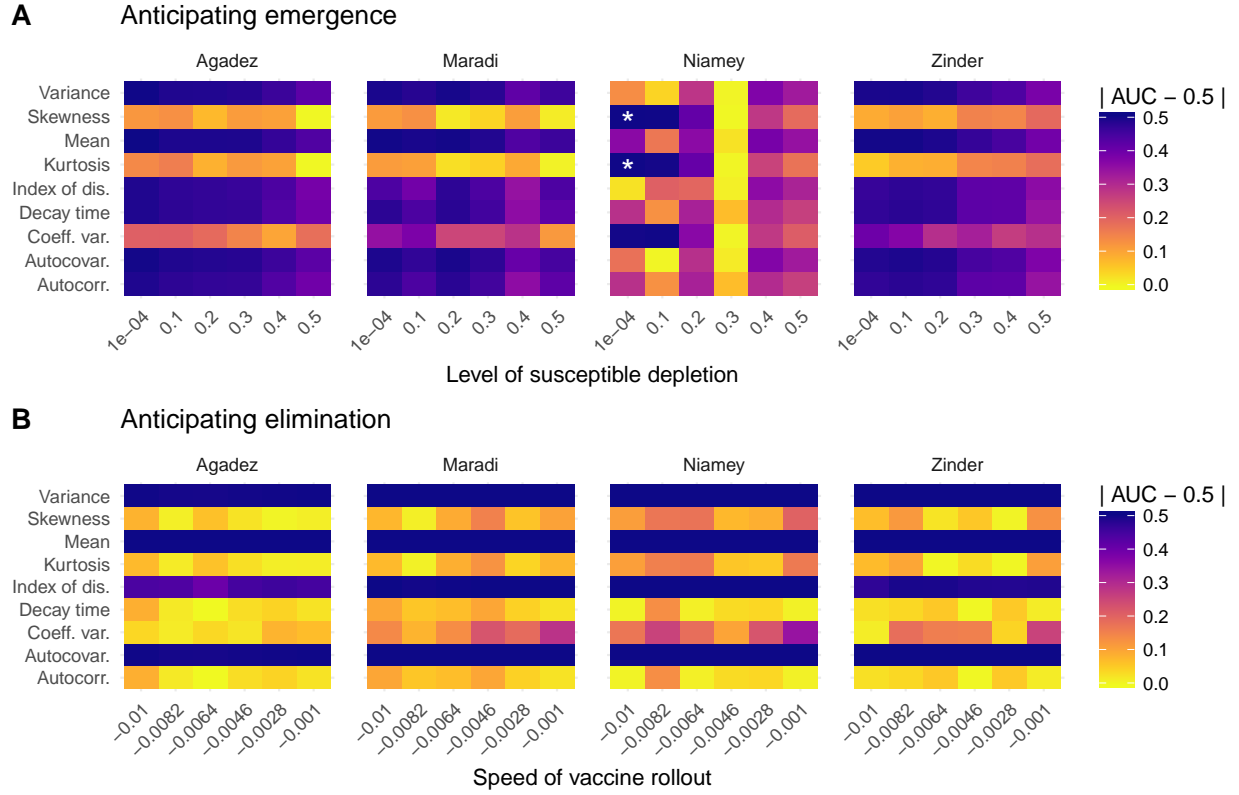


**Figure 4:** Performance of EWS calculated over two windows (far from and near  $R_E(t) = 1$ ) from the time series of 500 simulated dynamics, shown as a heatmap of AUC values minus 0.5. The two windows were defined as equally-sized windows over the course of the time series up to  $R_E(t) = 1$  (red lines in Figure 3). The asterisks (\*) in the heatmap for Niamey note EWS with high AUC, but for the wrong reason: skewness and kurtosis *decrease* as  $R_E(t)$  approaches 1 rather than increase. This occurs because of the negative binomial sampling in the measurement component of our SEIR model.

Journal of the Royal Society Interface 13:20160540.

Ferrari, M. J., R. F. Grais, N. Bharti, A. J. Conlan, O. N. Bjørnstad, L. J. Wolfson, P. J. Guerin, A. Djibo, and B. T. Grenfell. 2008. The dynamics of measles in sub-Saharan Africa. *Nature* 451:679–684.

Han, B. A., and J. M. Drake. 2016. Future directions in analytics for infectious disease intelligence. *EMBO reports*:e201642534.

Ionides, E. L., C. Breto, J. Park, R. A. Smith, and A. A. King. 2017. Monte Carlo profile confidence intervals for dynamic systems. *Journal of the Royal Society Interface* 14:20170126.

Ionides, E. L., D. Nguyen, Y. Atchadé, S. Stoev, and A. A. King. 2015. Inference for dynamic and latent variable models via iterated, perturbed Bayes maps. *Proceedings of the National Academy of Sciences* 112:719–724.

King, A. A., E. L. Ionides, C. M. Breto, S. P. Ellner, M. J. Ferrari, B. E. Kendall, M. Lavine, D. Nguyen, D. Reuman, H. Wearing, and S. N. Wood. 2018. pomp: Statistical Inference for Partially Observed Markov Processes (R package, version 1.18).

King, A. A., D. Nguyen, and E. L. Ionides. 2016. Statistical Inference for Partially Observed Markov

Processes via the R Package pomp. *Journal Of Statistical Software* 69:1–43.

O’Dea, E. B. 2018. spaero: Software for Project AERO (R package version 0.3.0).

R Core Team. 2017. R: A language and environment for statistical computing.

Robin, X., N. Turck, A. Hainard, N. Tiberti, F. Lisacek, J.-C. Sanchez, and M. Müller. 2011. pROC: an open-source package for R and S+ to analyze and compare ROC curves. *BMC Bioinformatics* 12:77.